Takahashi *et al. Earth, Planets and Space* (2019) 71:87
https://doi.org/10.1186/s40623-019-1066-y

Earth, Planets and Space

EXPRESS LETTER

Open Access

Underground structures associated with horizontal sliding at Uchinomaki hot springs, Kyushu, Japan, during the 2016 Kumamoto earthquake

Kosuke Takahashi[1], Takeshi Tsuji[1,2*], Tatsunori Ikeda[2], Hiro Nimiya[1], Yuichiro Nagata[1] and Yudai Suemoto[1]

Abstract

The 2016 Kumamoto earthquake (Mw 7.0) caused hot springs in the Uchinomaki area of Aso caldera to become dormant. Geodetic and borehole observations have previously demonstrated that the area around the hot springs slid horizontally ~ 2 m to the northwest during the earthquake. However, the subsurface structure in the area has not been investigated and the mechanism of sliding is unclear. To reveal geological structures in and around the hot spring area, we conducted a seismic microtremor survey at 60 sites and used the Extended Spatial Auto Correlation (ESPAC) method to determine surface-wave dispersion curves from the microtremor data. We then derived S-wave velocity profiles by inversion of the dispersion curves and constructed from them a 3D S-wave velocity model to ~ 100 m depth over the hot springs and surrounding areas. New surface fissures (indicative of extension) that opened during the 2016 earthquake correspond to a boundary in the southeast of the study area between modeled lower velocities (to the northwest) and higher velocities (to the southeast). In the central area of the hot springs, where the largest displacement occurred, the 3D model shows a plume-like high-velocity anomaly, indicative of more-competent sediments there. The lowest S-wave velocities (less-competent rocks) are in paddy fields north of the hot spring area. We interpret the above aspects of the 3D velocity model to indicate that during the 2016 earthquake the relatively competent (higher S-wave velocity) sediments in the central area of the hot springs slid northwestward, causing compressional deformation of the less-competent (lower S-wave velocity) sediments in the northern paddy fields and extensional deformation (fissures) southeast of the sliding block. A distinct increase in S-wave velocity at ~ 50 m depth coincides with the depth of a pumice layer in drillcore from the central hot spring area. Shaking during the 2016 earthquake could have caused a sudden increase in pore pressure in this widely distributed porous layer, thus providing a slip plane for the observed horizontal sliding to the northwest.

Keywords: 2016 Kumamoto earthquake, Horizontal sliding, Microtremor array measurement, Spatial autocorrelation, 3D geological model

*Correspondence: tsuji@i2cner.kyushu-u.ac.jp
[1] Department of Earth Resources Engineering, Kyushu University, 744 Motooka, Nishi-ku, Fukuoka 819-0395, Japan
Full list of author information is available at the end of the article

Introduction

The 2016 Kumamoto earthquake caused serious damage over a wide area of central Kyushu Island, Japan. The foreshock (Mw 6.2) was on the Hinagu fault on 14 April 2016 and the main shock (Mw 7.0) was on the Futagawa fault on 16 April (Fig. 1a) (e.g., Asano and Iwata 2016; Kato et al. 2016). The earthquake caused large crustal deformation, and new movements on many exposed faults were observed (Geological Survey of Japan 2016; Shirahama et al. 2016; Nakano et al. 2016a). In the Uchinomaki area northwest of Aso caldera (Fig. 1b), hot spring production ceased at some wells. Investigations after the earthquakes (Fujiwara et al. 2017; Nakano et al. 2016b; Tsuji et al. 2017) included satellite data analyses (e.g., Differential Interferometric Synthetic Aperture Radar Interferometry; DInSAR), downhole logging including borehole photography and drillcore inspections, and field observations. DInSAR analyses (Fujiwara et al. 2017; Tsuji et al. 2017) showed that the land surface in the Uchinomaki area had moved ~2 m to the northwest during the earthquakes. Drill strings at several well sites were bent, and borehole casings were broken at ~50 m depth during the earthquake (Tsuji et al. 2017). Several new extensional fissures had developed in the southeastern part of the deformed area (purple lines in Fig. 1c) and evidence of compressional deformation was observed on the northern side of the hot spring area (red squares in Fig. 1c; Tsuji et al. 2017). These results suggest that horizontal sliding had occurred along a geological unit at ~50 m depth, moving the entire ~2-km-diameter Uchinomaki hot spring area ~2 m northwestward (Tsuji et al. 2017).

The above studies were based on surface information and localized observations from wells in the area, so the 3D perspective of subsurface changes of the geological structure at the Uchinomaki hot springs has not been explored and the mechanism of horizontal sliding has not been clearly elucidated. Although there have been many studies of landslides and lateral movements caused by earthquakes (e.g., Sassa et al. 1996; Keefer 2002; Chigira et al. 2003; Chigira and Yagi 2006), horizontal sliding has rarely been investigated in low-relief plains such as the Uchinomaki area (Fig. 1). In this study, we conducted a microtremor seismic survey in the Uchinomaki area (white dots in Fig. 1c) and constructed a 3D S-wave velocity model from the surface to 100 m depth. Our results clearly reveal a relationship between the subsurface structure and the area of horizontal sliding.

Data

We conducted our microtremor array survey at ~60 points in and around the Uchinomaki hot spring area (white dots in Fig. 1c) using an L-shaped array of nine seismometers (Additional file 1: Fig. S1a). One seismometer was placed at the center of the array, with four seismometers placed on each of the limbs of the array. At observation points where the available space for seismometer deployment was limited, we used arrays

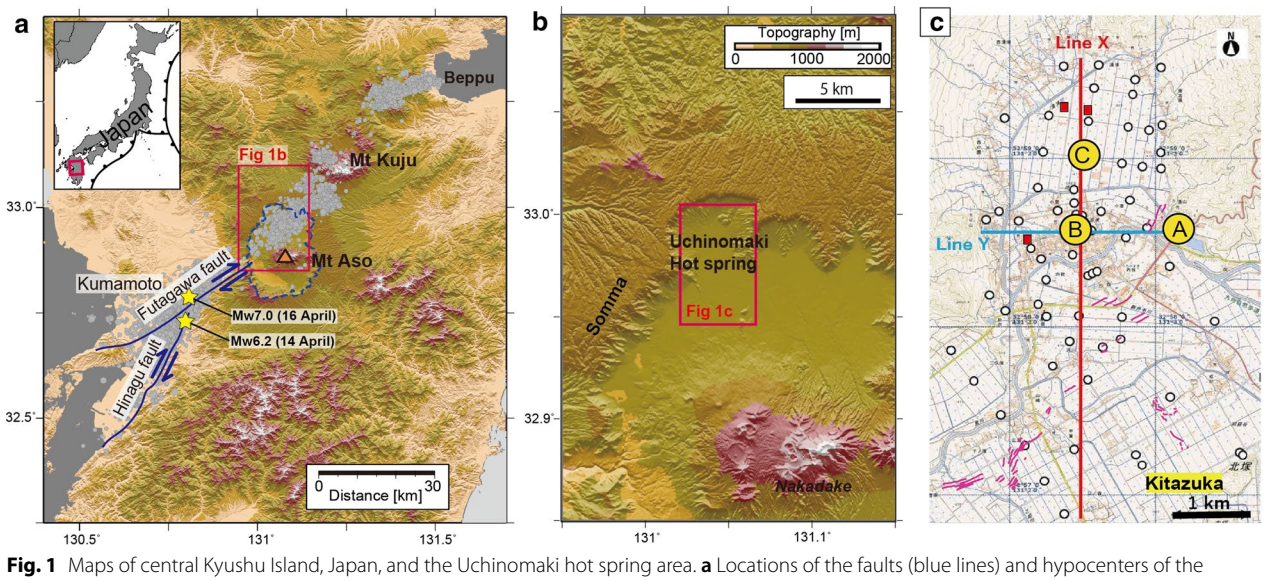

Fig. 1 Maps of central Kyushu Island, Japan, and the Uchinomaki hot spring area. **a** Locations of the faults (blue lines) and hypocenters of the foreshock and mainshock (yellow stars) and aftershocks (gray dots) of the 2016 Kumamoto earthquake are shown (modified from Tsuji et al. 2017). The dashed line outlines Aso caldera. **b** Enlarged map around the Uchinomaki hot spring area. **c** Positions of microtremor arrays (white dots). Purple lines represent open fissures revealed by field observations and interpretations of satellite data (Tsuji et al. 2017). We used the 10-m mesh digital elevation model (DEM) in **a**, **b**, and regional map in **c** published by the Geospatial Information Authority of Japan (http://www.gsi.go.jp/)

of different sizes or shapes. Louie (2001) showed that S-wave velocity structures can be obtained even by linear arrays if a small frequency range between 1 and 10 Hz is used. Moreover, Hayashi et al. (2006) have demonstrated that irregular arrays can be effective for the determination of S-wave velocities.

We used a wireless seismometer system (vertical component) with recording time synchronized by GPS. Microtremor data were recorded with a 4 ms sample interval for ~20 min at each observation point (Additional file 1: Fig. S1b). When the microtremor data were unstable, we recorded for a longer duration (e.g., ~30 min).

Method

Dispersion curves are commonly obtained from array measurements of microtremors using the Spatial Auto Correlation (SPAC) method (e.g., Aki 1957; Okada 2003; Asten 2006) or the frequency–wavenumber (*f*–*k*) method (Capon 1969; Lacoss et al. 1969). We used the Extended Spatial Auto Correlation (ESPAC) method (Ling and Okada 1993; Okada 2003) because previous studies have demonstrated that this method provides more reliable estimates of dispersion curves than the *f*–*k* method (e.g., Ohori et al. 2002; Foti et al. 2011). The ESPAC method defines the real parts of cross-coherence as SPAC coefficients and expresses them theoretically using the zero-order Bessel function of the first kind, as follows:

$$\rho(f, \Delta x) = J_0\left(\frac{2\pi f}{V(f)}\Delta x\right), \tag{1}$$

where ρ is the SPAC coefficient, f frequency, Δx receiver spacing, $V(f)$ phase velocity, and J_0 the zero-order Bessel function of the first kind.

To estimate dispersion curves, we computed root-mean-square errors (RMSEs) between the observed SPAC coefficient and the Bessel function as defined in Eq. (1) (Additional file 1: Fig. S1c). Dispersion curves at each frequency were then obtained by extracting the data point with the lowest RMSE (dots in Additional file 1: Fig. S1c). The frequency range of the dispersion curve was defined by the following relationship between wavelength and receiver spacing.

$$2\Delta x_{\min} < \lambda < 2\Delta x_{\max}, \tag{2}$$

where $\lambda = \frac{V(f)}{f}$ is wavelength, $\Delta x_{\min}$ the minimum receiver spacing, and $\Delta x_{\max}$ the maximum receiver spacing. We manually picked phase velocities considered to be a fundamental mode of Rayleigh waves within the frequency range.

We performed inversion analysis of the resultant dispersion curve to determine the subsurface S-wave velocity structure (Additional file 1: Fig. S1d). The theoretical dispersion curve was calculated by the compound matrix method (Saito and Kabasawa 1993) based on the assumption that the subsurface under the array is in the form of a horizontal multi-layered structure. As the initial model for inversion, we constructed S-wave velocity models by converting phase velocity and wavelength into S-wave velocity and depth by the Ballard method (Ballard 1964) as follows:

$$V_s = 1.1 \times V(f), \tag{3}$$

$$D = \frac{\lambda}{3}, \tag{4}$$

where V_s is S-wave velocity and D depth. We used 5 layers when the maximum depth computed from Eq. (4) is shallower than 50 m. However, when the maximum depth is deeper than 50 m, we used more layers. Thicknesses of each layer were defined so as they increase constantly with depth. Then, we minimized the residual between the observed and theoretical dispersion curves of the assumed S-wave velocity structure using five iterations of the non-linear least-squares method (e.g., Xia et al. 1999). During inversion, we searched only the S-wave velocity for those layers; P-wave velocities and densities were computed from S-wave velocities using the empirical equations of Kitsunezaki et al. (1990) and Ludwig et al. (1970), respectively.

Because the size of the array and the underground structure differ from each observation point, the frequency range of estimated phase velocities (i.e., investigation depth) varied. To clarify the spatial geological structure, we constructed a 3D S-wave velocity structure by interpolating among the inverted S-wave velocity structures at each observation point. For 3D interpolation, we used the Natural Neighbor Method (Sibson 1981), based on Voronoi tessellation of a discrete set of spatial points. This interpolation method has advantages over simpler methods of interpolation, such as nearest-neighbor interpolation, because it provides a smoother approximation of the underlying real function. To perform the interpolation, we first inserted the 3D S-wave velocity data into a volume of 3D grid cells (446 × 304 × 101 cells in the north–south, east–west, and vertical directions, respectively), which covered our study area. Cell dimensions were 10 m (horizontal) and 1 m (vertical), so the total dimensions of the volume were ~5 km north–south, ~3 km east–west, and 100 m deep, sufficient to cover the ~2-km-diameter displaced area. We did not extrapolate the velocity data to the edges of the 3D volume, and fixed S-wave velocities at 0 m (100 m/s) and 100 m depth (300 m/s). These S-wave velocities at boundaries were derived from *N*-values

obtained from boreholes in the study area. To clarify the resolution of our model, we performed checkerboard tests (Additional file 1: Fig. S2). Because the input velocity model is recovered in the checkerboard tests, we can interpret the subsurface structures identified in the 3D model.

Results and interpretation

Characteristic dispersion curves and S-wave velocity profiles obtained at locations A, close to the somma of Mount Aso; B, in the central area of Uchinomaki hot springs; and C, in a paddy field north of the springs, are shown in Fig. 2 (locations in Fig. 1c). North–south and east–west profiles and depth slices extracted from the 3D S-wave velocity volume are shown in Fig. 3. The 3D S-wave velocity model allowed us to recognize and characterize several geological features. High S-wave velocities near the somma of Mount Aso were shallower than elsewhere in the study area. For example, at point A near the somma (Fig. 1c), the high-velocity geological formation is as shallow as 20 m (Fig. 2b). The depth slices (Fig. 3d–f) show that the area of high S-wave velocity at the somma, which is composed of consolidated igneous rocks, has higher S-wave velocities than other areas. Although there is no somma on the southern side of the study area, a volcanic hill there ("Kitazuka" in Fig. 1c) shows high S-wave velocities (Fig. 3a), indicating that the Uchinomaki hot spring area is almost completely surrounded by igneous rocks (Fig. 3e), and that the low-velocity sedimentary rocks extend only to the southwestern edge of the study area, which is where new open fissures were observed after the 2016 earthquake (purple lines in Fig. 1c).

The lowest S-wave velocity was modeled in an area of paddy fields to the north of the Uchinomaki area (location C in Figs. 1c, 2b, 3). At this location, the modeled S-wave velocity was remarkably low (~60 m/s; Fig. 3a) and extended to ~25 m depth, which can be attributed to this area previously being a bog composed of soft sediments of high porosity, as described in the following. Aso caldera attained its current shape ~70 ka (Miyabuchi 2009) and in the Uchinomaki area, it has since been a basin-shaped structure, within which a caldera lake formed. Unconsolidated sediments were deposited in the lake, which subsequently dried up and formed a flat bog of low S-wave velocity (Hase et al. 2010; Fujiwara et al. 2017). Dispersion curves obtained at locations in the paddy fields were typically poorly defined mainly because surface waves are highly attenuated in sediments of such high porosity. Moreover, because the ESPAC method

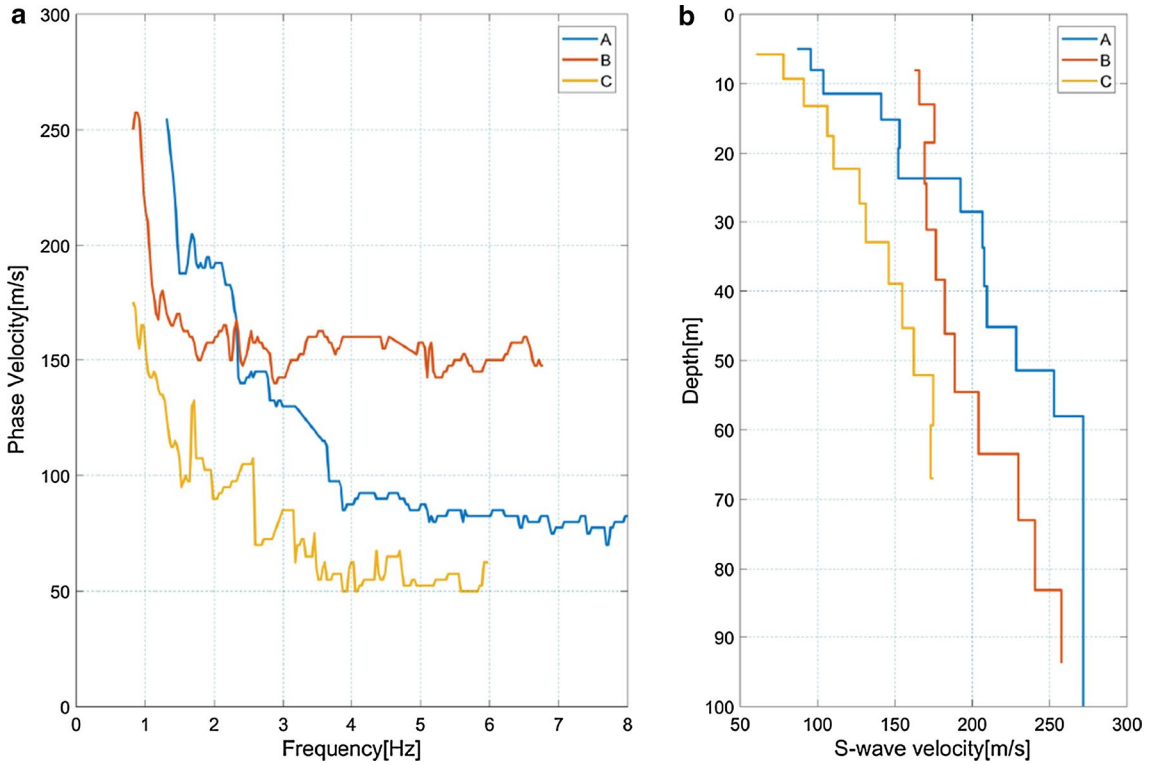

Fig. 2 **a** Phase velocity dispersion curves and **b** S-wave velocity–depth profiles at locations A, B, and C (see Fig. 1c for locations)

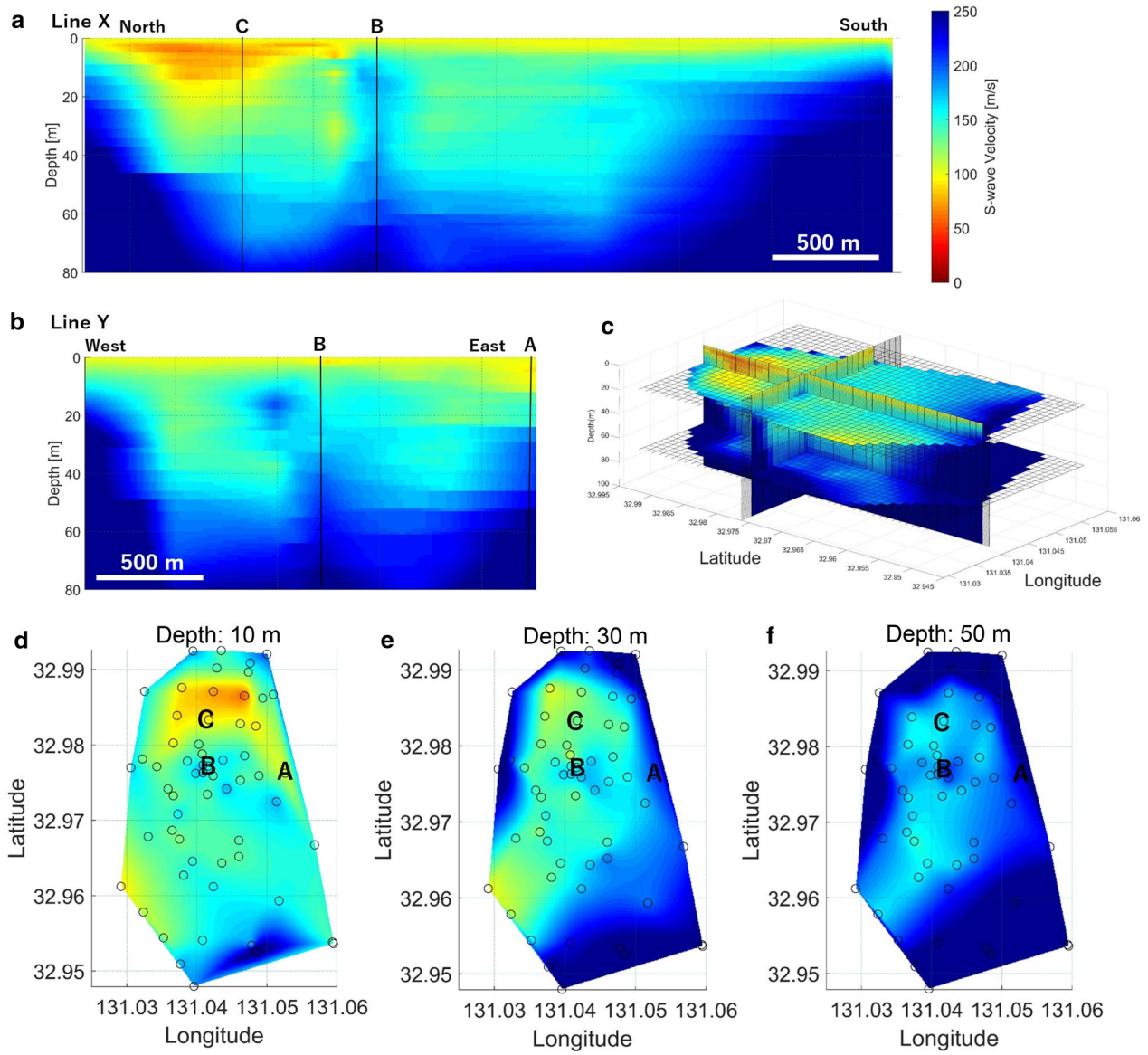

Fig. 3 S-wave velocity–depth profiles of **a** north–south Line X and **b** east–west Line Y (see Fig. 1c for locations). **c** Entire 3D S-wave velocity model constructed by interpolation of velocities estimated at array locations. Depth slices extracted from the 3D S-wave velocity model at **d** 10 m, **e** 30 m, and **f** 50 m

assumes a horizontally homogeneous structure (Okada 2003), lateral heterogeneity (e.g., fractures) within an array length could hamper estimation of dispersion curves (Andajani et al. 2019). Dispersion curves in the paddy fields were unclear especially near the boundary of horizontal sliding that Tsuji et al. (2017) identified, because of its lateral heterogeneity (Fig. 4c).

In the central part of the Uchinomaki hot spring area (location B in Figs. 1c, 2b, 3, 4), the shallow S-wave velocities are higher than in the surrounding area and take the form of a high-velocity plume-like shape rising from depth (Fig. 3a, b). Because this high-velocity feature is in the central area of the hot springs and in stratified sedimentary formation, one of the interpretations is that mineralization by hydrothermal fluids has influenced the physical and elastic properties of the sediments. If mineral precipitation occurred in the hot spring reservoir, a plume-like structure with high S-wave velocities might have developed. We therefore suggest that the high-velocity zone was formed by mineral precipitation due to the rise of hydrothermal fluids from the hot spring reservoir, forming

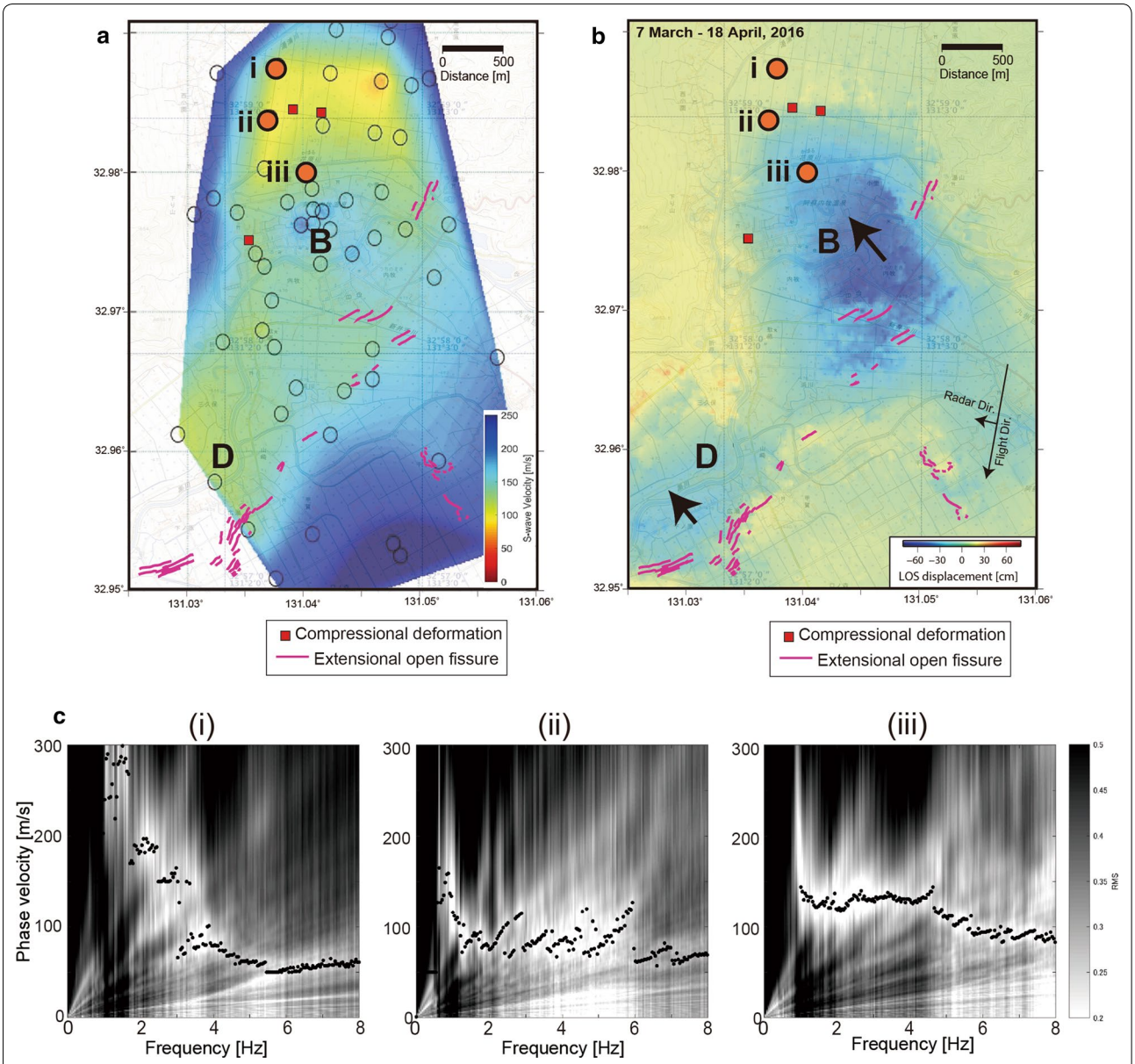

Fig. 4 Comparison of **a** S-wave velocity at 20 m depth and **b** surface deformation derived from DInSAR data (right-looking during descending orbits) from 7 March to 18 April 2016 (Tsuji et al. 2017). Purple lines represent open fissures interpreted from field observations and satellite data (Tsuji et al. 2017) and correspond to the northwestern boundary of the southern high-velocity region (**a**). The area of greatest displacement in **b** is in the area of the plume-shaped high-velocity anomaly near the center of the hot springs. **c** Comparison of dispersion curve at (i) northern paddy fields, (ii) compressional deformation area (fracture zone), and (iii) center of the hot spring (higher velocity). The locations of these survey positions are shown in **a**, **b**

more-competent beds. Indeed, in the past the hot spring reservoir beneath the center of the Uchinomaki hot spring area was shallower (~ 50 m depth) than the present reservoir (~ 200 m depth) (Tanaka 2000).

Discussion

A previous study has demonstrated that a geologic block of ~ 2 km breadth and width slid horizontally northwestward in the hot spring area during the mainshock of the 2016 Kumamoto earthquake (Tsuji et al. 2017). The sliding opened numerous new fissures ~ 1 m wide and aligned northeast–southwest along the southeastern edge of the block (purple lines in Fig. 4a, b). Those fissures are clearly spatially related to the northwestern boundary of the area of high S-wave velocities we derived from our microtremor data. Thus, horizontal sliding is related to the lithological boundary. The alignment of the dispersion curves we derived from our microtremor data across

the fracture zone is unclear, likely because of the heterogeneity of the sedimentary formations there (Ikeda and Tsuji 2016; Andajani et al. 2019). We obtained similarly unclear dispersion curves in an area of compressional deformation north of the area of the sliding geological block in the hot spring area (Fig. 4c).

An area to the southwest of the central Uchinomaki hot springs (location D in Fig. 4a, b) revealed by DInSAR data to have been displaced to the northwest (Tsuji et al. 2017) corresponds to an area of lower S-wave velocities. However, the geological block with the greatest displacement in the study area (location B in Fig. 4a, b; darker blue in Fig. 4b) is clearly spatially related to the area of higher S-wave velocity in the region of the plume-like feature we identified. As described above, this area likely contains more-competent units due to mineral precipitation or other reactions/alterations in the hydrothermal reservoir. Therefore, we suggest that the area of more-competent lithology slid farther to the northwest during the earthquake, because the softer sediments to the north could fail to resist the lateral forces due to earthquake vibration (i.e., dynamic stress during the earthquake) or the gravitational forces of the sliding block, which indicates that the horizontal sliding was largely controlled by the elastic properties (competence) of the sediments.

Borehole logs (natural gamma ray) from the interpreted area of sliding indicate a downward lithology transition at ~50 m depth (Fig. 5). This observation is supported by a widespread downward increase in S-wave velocity at about the same depth within the central part of the area of hot springs. This boundary might represent the horizontal sliding surface of the kilometer-scale geologic block. Several cores in this area penetrated layers of pumice at ~50 m depth (Tsuji et al. 2017). During the 2016 earthquake, the pore pressure in such porous layers beneath the low-permeability mud may have increased (Sassa et al. 1996), thus lowering friction and allowing horizontal sliding of the overlying sequence (Tsuji et al. 2014). Therefore, during the 2016 earthquake, the more-competent sediments in the central Uchinomaki area slid northward on the surface of the pumice layer (high pore pressure) at 50 m depth toward less-competent sediments, rather than toward the more-competent sediments to the south.

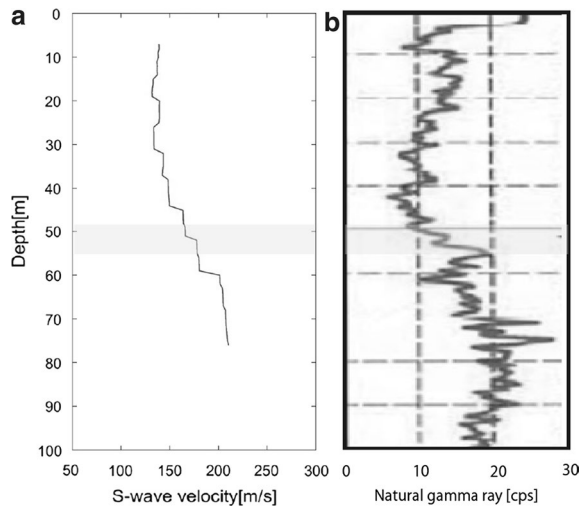

Fig. 5 Comparison of **a** S-wave velocity profile and **b** natural gamma ray log data measured at the same location (close to position B in Fig. 1c). The gray-shaded zone indicates the depth of the interpreted sliding surface

Conclusions

We used the results of a seismic microtremor survey to examine 3D spatial variations of S-wave velocity to a depth of ~100 m in the study area and to elucidate the mechanism of the horizontal northwestward displacement of the Uchinomaki area during the 2016 Kumamoto earthquake. Our findings are summarized below.

1. We revealed the existence of consolidated rock along the somma of Mount Aso, soft caldera lake sediments under the plain to the north of the Uchinomaki hot springs, and relatively high S-wave velocities within a plume-shaped anomaly under the central part of the hot spring area.
2. Numerous new fissures at the southern edge of the northward-sliding geological block are clearly spatially related to the boundary between higher and lower S-wave velocities, suggesting that horizontal sliding is related to the lithological boundary.
3. The dispersion curves we estimated in the paddy fields north of the central hot spring area and in the south where open fissures formed during the 2016 earthquake were unclear, likely because of subsurface heterogeneity at the sliding surface. Indeed, seismic velocities varied in the area where there were open fissures.
4. We modeled a considerable and widespread increase of S-wave velocity at ~50 m depth in the central area of the hot springs. We interpret this velocity discontinuity to represent the formation boundary along which the horizontal sliding of the kilometer-scale geologic block occurred.
5. During the 2016 earthquake, the more-competent rocks (high S-wave velocities) slid northward toward less-competent (lower S-wave velocity) sediments because they were incapable of resisting the lateral and gravitational forces imposed by the sliding geological block. The more-competent rocks in the south of the study area were capable of resist-

ing those forces. Similar geologic movements might occur during future strong earthquakes in or near the study area, or in areas where there are lithological boundaries similar to that we identified at ~ 50 m depth.

Additional file

Additional file 1. Additional figures.

Acknowledgements
This study received considerable support (accommodation for geophysical survey during several weeks) from the Association of Aso Hot Springs. K. Hayashi (Geometrics Inc.) and T. Yoshioka (OYO Corporation) supported data acquisition during the field survey.

Authors' contributions
TT proposed, conceived, and designed the study. KT, TT, TI, HN, YN, and YS participated in the field survey in 2016–2018 and data analysis. TT and TI supervised survey and data analysis. KT and TT mainly wrote the manuscript. All authors read and approved the final manuscript.

Funding
This work was supported by Grants-in-Aid for Scientific Research in Innovative Areas (JP17H05318) from the Japan Society for the Promotion of Science (JSPS).

Availability of data and materials
The microtremor data used in this study are available from the corresponding author on request.

Competing interests
The authors declare that they have no competing interests.

Author details
[1] Department of Earth Resources Engineering, Kyushu University, 744 Motooka, Nishi-ku, Fukuoka 819-0395, Japan. [2] International Institute for Carbon–Neutral Energy Research (WPI-I2CNER), Kyushu University, 744 Motooka, Nishi-ku, Fukuoka 819-0395, Japan.

Received: 2 February 2019 Accepted: 26 July 2019
Published online: 07 August 2019

References

Aki K (1957) Space and time spectra of stationary stochastic waves, with special reference to microtremors. Bull Earth Res Inst 35:415–456
Andajani RD, Ikeda T, Tsuji T (2019) Surface wave analysis for heterogeneous geological formation in geothermal field: Consideration of wave propagation direction, Exploration Geophysics, accepted
Asano K, Iwata T (2016) Source rupture processes of the foreshock and mainshock in the 2016 Kumamoto earthquake sequence estimated from the kinematic waveform inversion of strong motion data. Earth Planets Space 68:147
Asten MW (2006) On bias and noise in passive seismic data from finite circular array data processed using SPAC methods. Geophysics 71:V153–V162
Ballard RF Jr (1964) Determination of soil shear moduli at depth by in situ vibratory techniques, US Army Engineer Waterways Experiment Station, Vicksburg, Miss., Misc. Paper, No. 4-691
Capon J (1969) High-resolution frequency–wavenumber spectrum analysis. Proc IEEE 57:1408–1418. https://doi.org/10.1109/PROC.1969.7278
Chigira M, Yagi H (2006) Geological and geomorphological characteristics of landslides triggered by the 2004 Mid Niigta prefecture earthquake in Japan. Eng Geol 82:202–221
Chigira M, Wang WN, Furuya T, Kamai T (2003) Geological causes and geomorphological precursors of the Tsaoling landslide triggered by the 1999 Chi-Chi earthquake, Taiwan. Eng Geol 68:259–273
Foti S, Parolai S, Albarello D, Picozzi M (2011) Application of surface-wave methods for seismic site characterization. Surv Geophys 32:777–825. https://doi.org/10.1007/s10712-011-9134-2
Fujiwara S, Morishita Y, Nakano T, Kobayashi T, Yarai H (2017) Non-tectonic liquefaction-induced large surface displacements in the Aso Valley, Japan, caused by the 2016 Kumamoto earthquake, revealed by ALOS-2 SAR. Earth Planet Sci Lett 474:457–465
Geological Survey of Japan (2016) Surface earthquake faults associated with the 2016 Kumamoto earthquake. https://www.gsj.jp/hazards/earthquake/kumamoto2016/kumamoto20160513-1.html. Accessed 15 July 2018
Hase Y, Miyabuchi Y, Haruta N, Sasaki N, Yumoto T (2010) Change of sedimentary facies and topographic process after the late period of the Last Glacial Age of Asodani in the northern area of Aso Caldera in Central Kyushu, Japan. Bull Goshoura Cret Mus 11:1–10 **(in Japanese with English abstract)**
Hayashi K, Inazaki T, Suzuki H (2006) Buried incised-channels delineation using microtremor array measurements at Soka and Misato Cities in Saitama Prefecture. Bull Geol Surv Jpn 57(9/10):309–325
Ikeda T, Tsuji T (2016) Surface wave attenuation in the shallow subsurface from multichannel–multishot seismic data: a new approach for detecting fractures and lithological discontinuities. Earth Planets Space 68:111. https://doi.org/10.1186/s40623-016-0487-0
Kato A, Fukuda J, Nakagawa S, Obara K (2016) Foreshock migration preceding the 2016 Mw 7.0 Kumamoto earthquake, Japan. Geophys Res Lett 43:15
Keefer DK (2002) Investigating landslides caused by earthquakes—a historical review. Surv Geophys 23:473–510
Kitsunezaki C, Goto N, Kobayashi Y et al (1990) Estimation of P-and S-wave velocities in deep soil deposits for evaluating ground vibrations in earthquake (in Japanese). J Jpn Soc Nat Disast Sci 9–3:1–17
Lacoss RT, Kelly EJ, Toksöz MN (1969) Estimation of seismic noise structure using arrays. Geophysics 34:21–38. https://doi.org/10.1190/1.1439995
Ling S, Okada H (1993) An extended use of the spatial autocorrelation method for the estimation of structure using microtremors. In: Proceedings of the 89th SEGJ Conference, 1993 October 12–14, Society of Exploration Geophysicists of Japan, Nagoya, Japan, 44–48
Louie JN (2001) Faster, better: shear-wave velocity to 100 meters depth from refraction microtremor arrays. Bull Seism Soc Am 91:347–364
Ludwig WJ, Nafe JE, Drake CL (1970) Seismic refraction. Sea 4:53–84
Miyabuchi Y (2009) A 90,000-year tephrostratigraphic framework of Aso Volcano, Japan. Sed Geol 220:169–189
Nakano T, Kobayashi T, Yoshida K, Fujiwara S (2016) Field Survey of Non-tectonic Surface Displacements Caused by the 2016 Kumamoto Earthquake Around Aso Valley. Bulletin of the Geospatial Information Authority of Japan, Vol. 64
Nakano T, Une H, Sekiguchi T, Sakai H, Yoshida K (2016) Distribution of surface cracks caused by the 2016 Kumamoto Earthquake interpreted from aerial photos. In: Paper presented at the Japan Geoscience Union meeting, Chiba, Japan, 22–26 May 2016 (MIS34-P55)
Ohori M, Nobata A, Wakamatsu K (2002) A comparison of ESAC and FK methods of estimating phase velocity using arbitrarily shaped microtremor arrays. Bull Seismol Soc Am 92:2323–2332. https://doi.org/10.1785/011998010 9
Okada H (2003) The Microtremor Survey Method, Geophysical Monograph, No. 12, Society of Exploration Geophysicists, Tulsa, OK
Saito M, Kabasawa H (1993) Computation of reflectivity and surface wave dispersion curves for layered media. 2: Rayleigh wave calculations (in Japanese). Butsuri-Tansa 46:283–298
Sassa K, Fukuoka H, Scarascia-Mugnozza G, Evans S (1996) Earthquake-induced-landslides: distribution, motion and mechanisms. Soils Found 36:53–64
Shirahama Y, Yoshimi M, Awata Y, Maruyama T, Azuma T, Miyashita Y, Mori H, Imanishi K, Takeda N, Ochi T, Otsubo M, Asahina D, Miyakawa A

(2016) Characteristics of the surface ruptures associated with the 2016 Kumamoto earthquake sequence, Kyushu, southwestern Japan. In: Paper presented at the Japan Geoscience Union meeting, Chiba, Japan, 22–26 May 2016 (MIS34-P45)

Sibson R (1981) A brief description of natural neighbor interpolation. In: Barnett V (ed) Interpreting multivariate data. Wiley, New York, pp 21–36

Tanaka N (2000) Nature and culture of Aso 8. Mount Aso and Water, Committee of editing history of Ichinomiya town

Tsuji T, Kamei R, Pratt G (2014) Pore pressure distribution of a mega-splay fault system in the Nankai Trough subduction zone: insight into up-dip extent of the seismogenic zone. Earth Planet Sci Lett 396:165–178. https://doi.org/10.1016/j.epsl.2014.04.011

Tsuji T, Ishibashi J, Ishitsuka K, Kamata R (2017) Horizontal sliding of kilometre-scale hot spring area during the 2016 Kumamoto earthquake. Sci Rep 7:42947. https://doi.org/10.1038/srep42947

Xia J, Miller RD, Park CB (1999) Estimation of near-surface shear-wave velocity by inversion of Rayleigh waves. Geophysics 64(3):691–700

Publisher's Note